Low △ 12 CH 2 D 2 values in microbialgenic methane result from combinatorial isotope effects

Lina Taenzer, Jabrane Labidi, Andrew L Masterson, Xiahong Feng, Douglas Rumble, Edward D Young, William D Leavitt

Low apparent $\Delta^{12}CH_2D_2$ in microbialgenic methane result from combinatorial isotope effects

Lina Taenzer[a], Jabrane Labidi[b], Andrew L. Masterson[c], Xiahong Feng[d], Douglas Rumble III[e], Edward D. Young[f], William D. Leavitt[g]

correspondence: william.d.leavitt@dartmouth.edu, eyoung@epss.ucla.edu

[a]*Department of Earth Sciences, Dartmouth College; Present Address: MIT-WHOI*
[b]*Department of Earth, Planetary, and Space Sciences, UCLA; Present Address: Institut de Physique du Globe de Paris*
[c]*Department of Earth & Planetary Sciences, Northwestern University*
[d]*Department of Earth Sciences, Dartmouth College*
[e]*The Geophysical Lab, Carnegie Institution for Science*
[f]*Department of Earth, Planetary, and Space Sciences, UCLA*
[g]*Department of Earth Sciences, Department of Biological Sciences, Department of Chemistry, Dartmouth College*

Abstract

Methane generated by microorganisms is most often depleted in the doubly substituted isotopologue $^{12}CH_2D_2$ relative to the stochastic reference distribution. To constrain the controls on depleted $\Delta^{12}CH_2D_2$ values, we experimentally isolated the root cause with microorganisms that produce methane from methylphosphonate via the C-P lyase pathway. This mechanism of methane production preserves the three hydrogens from methylphosphonate and adds one hydrogen from water. When maintaining the same methylphosphonate source, but varying the D/H composition of growth medium water, we observed significant shifts in methane $\Delta^{12}CH_2D_2$ values, but little to no change in $\Delta^{13}CH_3D$ values. We reproduced these observations with a model that considers only the combinatorial isotope effect. The variation in $\Delta^{12}CH_2D_2$ values of product methane resulted from the differences in D/H between reactants water and methylphosphonate. This work validates the hypothesis that combinatorial effects can strongly influence methane $\Delta^{12}CH_2D_2$ values, and must be considered for low temperature, abiotic or biotic systems where methane hydrogen is derived from multiple reservoirs.

Keywords: methane, clumped isotopes, methanogenesis, C-P lyase

1. Introduction

Multiply-substituted ("clumped") isotopologues are powerful tracers of molecular formation reactions (Eiler and Schauble, 2004; Stolper et al., 2014; Wang et al., 2015; Yeung et al., 2015; Young et al., 2017; Yeung et al., 2017; Popa et al., 2019). Exploring variations in the relative abundance of the two doubly-substituted mass-18 isotopologues of methane, $^{12}CH_2D_2$ and $^{13}CH_3D$, have provided promising constraints on provenance, even where bulk C and H isotopic ratios ($^{13}C/^{12}C$, D/H) yielded ambiguous information as to source and process (Young et al., 2017; Haghnegahdar et al., 2017; Young, 2019; Giunta et al., 2019; Ash et al., 2019). The relative abundance of the two mass-18 clumped isotopologues in a given population of methane molecules formed at high temperature ($\geq$ 1000 K) in thermodynamic equilibrium, are approximated by a random distribution of all possible isotopologue combinations. This apportioning of isotopes is referred to as a "stochastic distribution," and provides the reference frame for reporting the relative abundances of clumped isotopologues (Eiler and Schauble, 2004). The abundance of a given multiply-substituted isotopologue relative to the most abundant isotopologue (e.g. $^{13}CH_3D/^{12}CH_4$) is reported as a fractional difference from the stochastic relative abundances, Δ_i, where subscript i refers to the specific clumped species, and Δ_i are reported in permil (‰). This stochastic reference frame highlights whether a process has favored or discriminated against the formation of molecules with bonds containing multiple heavy isotopes (e.g., $^{13}CH_3D$), rather than only differences in bulk isotope ratios. Under equilibrium conditions at low temperatures ($<$ 300 K), the stability associated with bonds between heavy isotopes in a molecule increases, promoting the formation of the isotopically clumped molecular species. As temperature approaches infinity, this effect diminishes and the relative abundance of multiply-substituted molecules decreases, approaching $\Delta_i = 0$. Under non-equilibrium conditions at low temperatures, departures from the stochastic distribution may provide insights into the kinetics and reaction(s) of formation for a given methane population's natural history.

Methane produced by microorganisms is characterized by significant depletion or "anti-clumping" in the $\Delta^{12}CH_2D_2$ values by more than 20 to 50‰, relative to thermodynamic equilibrium (Young et al., 2017). These $\Delta^{12}CH_2D_2$ deficits are accompanied by negligible depletion in $\Delta^{13}CH_3D$ values (Figure 1). Several hypotheses have been put forward to explain these observed departures from thermodynamic equilibrium. The two hypotheses in the literature thus

far are: i) contributions from distinct pools of hydrogen with disparate D/H ratios and/or differentially fractionated H sites during formation, and ii) quantum tunneling of hydrogen during methane formation (Young et al., 2017; Yeung, 2016; Röckmann et al., 2016; Young, 2019; Cao et al., 2019). The former refers to the so-called "combinatorial effect." The importance of the combinatorial effect as a source of anti-clumping, wherein the measured clumped isotopologue abundance is less than predicted by theory, was first hypothesized during the study of molecular oxygen clumped isotopologues (Yeung et al., 2015; Yeung, 2016; Röckmann et al., 2016) and was suggested as relevant to microbially produced (microbialgenic) methane (Young et al., 2017). However, the combinatorial effect has not been directly tested or demonstrated in any experimental study. While this effect can arise from drawing on two or more reservoirs, it is not simply mixing in the general sense. To interpret the significance of depleted (anti-clumped) $\Delta^{12}CH_2D_2$ values requires a thorough understanding of if, when and how the combinatorial effect is expressed. This understanding is essential to the application of clumped isotope signatures as tracers of methane provenance, and extends to other gasses that could hypothetically experience combinatorics in altering the relative abundance of multiply substituted isotopologue ratios, such as molecular oxygen ($\Delta^{18}O^{18}O$) or dinitrogen ($\Delta^{15}N^{15}N$).

To experimentally test for the combinatorial effect and quantify its influence on $\Delta^{12}CH_2D_2$ values, we examined the bulk and clumped methane isotopologue abundances produced by bacteria operating the C-P lyase pathway. This microbialgenic methane production pathway is related to phosphorous acquisition and not core energy metabolism (White and Metcalf, 2004; Sosa et al., 2019), the canonical anaerobic microbial methanogens (Valentine, 2011). This metabolism provides a unique opportunity to study the combinatorial effect because this pathway incorporates hydrogen from two distinct reservoirs during methane formation: three from the methyl group of methylphosphonate and one from water (Kamat et al., 2011, 2013). Moreover, this methane is generated by rapidly growing bacteria where the bulk isotopic fractionations are independent of energy metabolism and growth rate (Taenzer et al., 2020). By varying the D/H composition of the water in which the bacteria grew and generated methane, we observed dramatic shifts in $\Delta^{12}CH_2D_2$ with minimal effect on $\Delta^{13}CH_3D$. Our experimental and model results together indicate that shifts in methane $\Delta^{12}CH_2D_2$ produced by the C-P lyase pathway were primarily due to the relative differences in D/H between water and methylphosphonate methyl hydrogens. The consistency

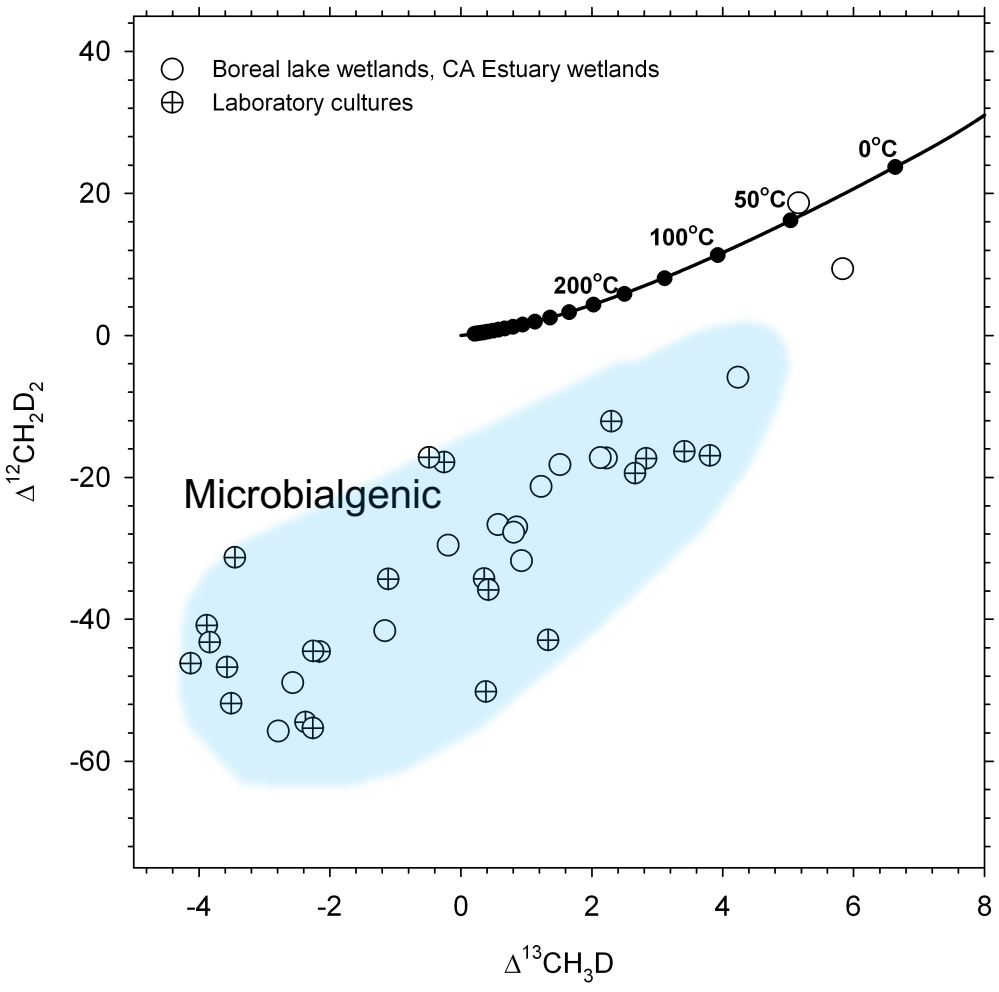

Figure 1: The distribution of laboratory axenic cultures (circles with crosses) and naturally-produced methane (open circles) by microbial methanogenesis in $\Delta^{12}CH_2D_2$ vs.$\Delta^{13}CH_3D$ space. The curve representing thermodynamic equilibrium is shown for reference, annotated with temperatures. Calculations and values are from Young (2019) and references therein.

between model predicted and experimentally generated isotopologue abundances demonstrates that the combinatorial effect can yield markedly negative $\Delta^{12}CH_2D_2$ values (below < -50‰) with little influence on $\Delta^{13}CH_3D$ values (<1‰). Implications for the interpretation of experimental and natural methane clumped isotopologue studies are discussed.

2. Principles of the Combinatorial Effect

The stochastic distribution is the reference frame for reporting multiply substituted (clumped) isotopologue abundances. It is defined by the most probable abundance of the multiply-substituted isotopologue of interest assuming that the isotopes comprising the molecules were randomly distributed among all possible isotopologues. The stochastic reference is calculated by equating fractional isotopic abundances with probabilities. To illustrate the essence of the combinatorial effect and for simplicity we examine cases for the formation of two diatomic molecules, carbon monoxide (CO) and molecular oxygen (O_2).

The stochastic distribution for the relative abundance of the multiply-substituted isotopologue $^{13}C^{18}O$ in a sample of carbon monoxide gas is calculated as

$$x(^{13}C^{18}O) = x(^{13}C)x(^{18}O) \tag{1}$$

where $x^{13}C$ is the fractional abundance of ^{13}C relative to all carbon isotopes by number (i.e., $^{13}C/(^{12}C +^{13} C)$), $x^{18}O$ is the fractional abundance of ^{18}O relative to all oxygen isotopes (i.e., $^{18}O/(^{16}O +^{17} O +^{18} O)$), and $x(^{13}C^{18}O)$ is the fractional abundance of the $^{13}C^{18}O$ isotopologue relative to all CO molecules. The ratio of this multiply-substituted isotopologue to the most abundant isotopic species is therefore $x(^{13}C^{18}O)/x(^{12}C^{16}O)$. It is common to express ratios of relative isotopologue fractions in terms of the isotope ratios of their constituent elements. In this case, $x(^{13}C^{18}O)/x(^{12}C^{16}O) = (^{13}C/^{12}C)(^{18}O/^{16}O) = {}^{13}R^{18}R$. Similarly, the stochastic fractional abundance of the multiply-substituted isotopologue of molecular oxygen (O_2) composed of two ^{18}O atoms is

$$x(^{18}O^{18}O) = x(^{18}O)x(^{18}O) \tag{2}$$

where the symbols are analogous to those in Equation 1. In this case $x(^{18}O^{18}O)/x(^{16}O^{16}O) = (^{18}O/^{16}O)(^{18}O/^{16}O) = {}^{18}R^2$.

For both $^{18}O^{18}O$ and $^{13}C^{18}O$, the accuracy of the estimated stochastic distribution is dictated by the fidelity of the bulk isotope ratios (e.g., $^{13}R = {}^{13}C/{}^{12}C$ and $^{18}R = {}^{18}O/{}^{16}O$) relative to these ratios at the time the molecules formed, and the degree to which the sample separation chemistry and mass-spectrometry can capture these ratios, free of subsequent fractionation effects. The cases of CO and O_2 represent contrasting examples of the ability to reconstruct the actual isotope ratios of the constituent atoms during assembly of the molecules. In the case of CO, the isotopic compositions of C and O unambiguously represent the isotope ratios of the constituent atoms since carbon and oxygen are distinguishable; the analysis of carbon monoxide yields $^{13}C/^{12}C$ and $^{18}O/^{16}O$ bulk ratios that faithfully record the actual isotopic compositions of the two constituent atoms (there is no confusing C and O, see Figure 2). In contrast, in the case of O_2, the isotopologue of interest is composed of two atoms of the same element and so the molecular positions can not be distinguished from one another. Therefore, despite the fact that the two atoms comprising the O_2 molecule may have originated from different reservoirs with distinct $^{18}O/^{16}O$ ratios (Yeung et al., 2015), the stochastic abundance of the $^{18}O^{18}O$ molecule is calculated on the basis of the average $^{18}O/^{16}O$ ratio. That is, the $^{18}O/^{16}O$ of the O_2 sample reflects an average of the two individual molecular sites and their source reservoirs. By necessity the $x(^{18}O^{18}O)\ /x(^{16}O^{16}O) = {}^{18}R^2$ value for the stochastic isotopologue ratio calculation assumes that the two molecular positions were formed from identical oxygen isotope ratios of ^{18}R. In reality, the oxygen isotope ratio is the average of two potentially distinct ratios,$^{18}R_1$ and $^{18}R_2$, which individually contributed to the O_2 molecule, such that:

$$[x(^{18}O^{18}O)/x(^{16}O^{16}O)]_{\text{stochastic}} = \left(\frac{(^{18}R_1 + {}^{18}R_2)}{2}\right)^2 \tag{3}$$

where subscripts 1 and 2 refer to two distinct oxygen reservoirs. The difference between using the actual constituent ratios $^{18}R_1{}^{18}R_2$ and using the average ratio $(^{18}R_1 + {}^{18}R_2)/2$ (by necessity) to calculate the stochastic ratio for the calculation of $\Delta^{18}O^{18}O$ is a manifestation of the mathematical truism that

$$(^{18}R_1)(^{18}R_2) \leq \left(\frac{(^{18}R_1) + (^{18}R_2)}{2}\right)^2. \tag{4}$$

In particular, we have for the true value for the fractional departure in

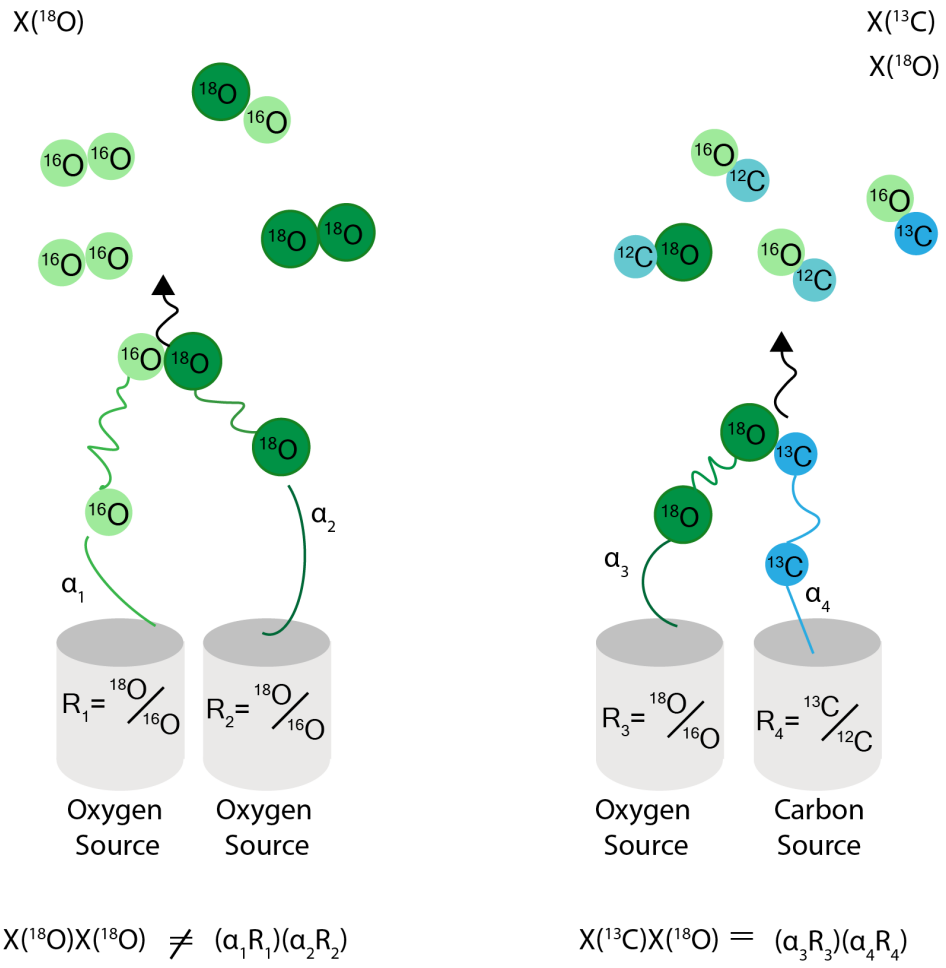

Figure 2: Schematic illustrations showing the pairing of oxygen-oxygen or oxygen-carbon isotopes when molecules of O_2 or CO are formed, respectively. The potential for two separate reactant reservoirs to contribute atoms from pools of distinct isotopic composition is illustrated for each case. For CO, the oxygen and carbon reservoirs are always distinguishable by virtue of their different elemental identities. The composition of the C and O sources are reflected in the isotopic ratios of the product CO, offset by any fractionation, which can be individually traced. On the contrary, in the case of two oxygen reservoirs contributing to O_2, only a single average isotopic composition can be determined for the product O_2 which obscures contributions from two separate, and potentially distinct oxygen sources and any fractionation between product and either of the sources.

$x(^{18}O^{18}O)/x(^{16}O^{16}O)$ from stochastic

$$\Delta^{18}O^{18}O = \frac{[x(^{18}O^{18}O)/x(^{16}O^{16}O)]_{\text{sample}}}{(^{18}R_1)(^{18}R_2)} - 1 \tag{5}$$

where "sample" refers to the measured isotopologue ratio. The $\Delta^{18}O^{18}O$ value from Equation 5 cannot be reconstructed *a priori*. Rather, the estimate obtained from the measured, average bulk isotopic composition of the O_2 gas itself is actually

$$\Delta^{18}O^{18}O = \frac{4[x(^{18}O^{18}O)/x(^{16}O^{16}O)]_{\text{sample}}}{\left((^{18}R_1) + (^{18}R_2) \right)^2} - 1. \tag{6}$$

Only when $^{18}R_1 = {}^{18}R_2$ will the two estimates be equal. Since the left-hand side of Equation 4 is the square of the geometric mean and the right-hand side is the square of the arithmetic mean, the inequality in this simple example is an expression of the well-known inequality of the geometric and arithmetic means, and is a general result (Yeung, 2016). Comparing Equations 4, 5, and 6 illustrates the general principle that when molecular positions are indistinguishable, and the average isotope ratios rather than the site-specific isotope ratios are all that is available for calculating the stochastic distribution of a multiply-substituted isotopologue, the stochastic abundance of the isotopologue i is overestimated, resulting in a spuriously low Δ_i value. The spuriously low and even negative Δ_i values are the result of the reference frame (Figure 3). Yeung and colleagues showed that for the case of multiply-substituted oxygen isotopologue in molecular oxygen that the measured $\Delta^{18}O^{18}O$ diverged drastically from the stochastic prediction (Yeung et al., 2015), and predicted that this is potentially due to two contributing sources (reservoirs) of isotopically distinct oxygen – that is, the combinatorial effect (Yeung, 2016). To date, however, no study has tested this experimentally for any other multiply substituted isotope system, be it oxygen, methane or another.

Given these examples above, we predict the combinatorial effect is possible whenever a molecule composed of multiple isotopes of the same element is constructed from more than one isotopic pool. The source of the different pools may result from different isotope effects for each step involved in constructing the molecule, or from drawing on isotopically distinct reservoirs. Candidates include, but are not limited to, multiply substituted isotopologues of N_2, O_2, H_2, CH_4, and N_2O. Despite the established theoretical

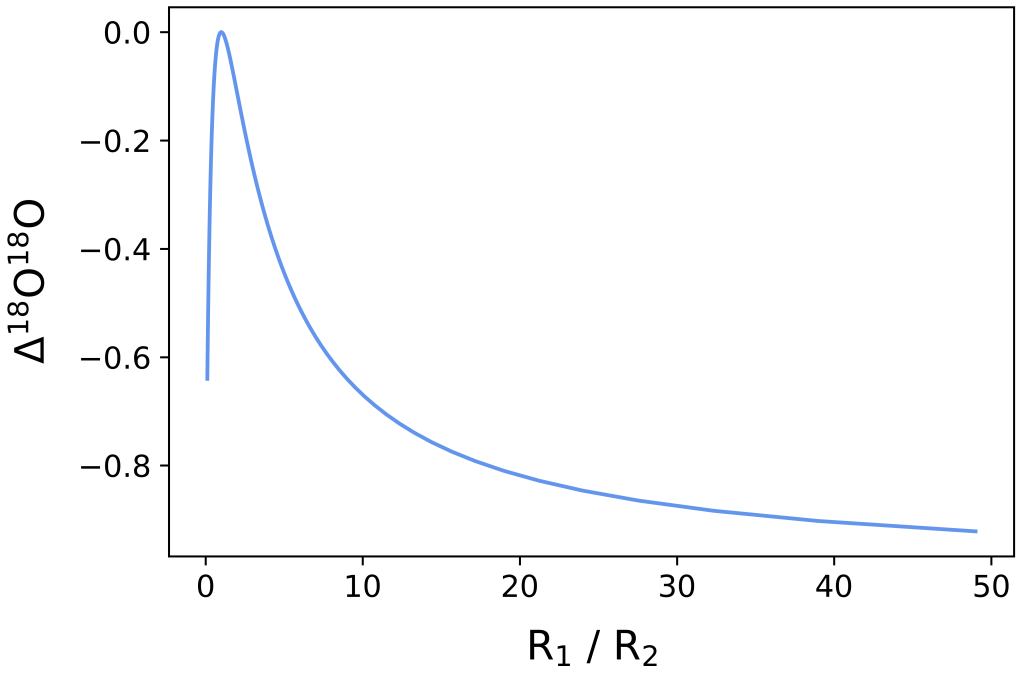

Figure 3: An illustration of the combinatorial effect seen when plotting $\Delta^{18}O^{18}O$ as a function of the ratio of the isotopic compositions, R_1 and R_2, of the distinct contributing oxygen reservoirs.

impact of combinatorics in influencing clumped isotopologue Δ_i values, it has yet to be demonstrated unambiguously in the laboratory. Substantiating the existence of the combinatorial effect and quantifying its magnitude are prerequisites to interpreting existing and future clumped isotopologue signatures in molecules composed of multiple atoms of the same element.

3. Methods

3.1. Microbial cultivation and gas production

The model microorganism *Pseudomonas stutzeri* strain HI00D01 (hereafter, strain HI00D01) was cultivated following the protocols in our recent study (Taenzer et al., 2020), with modifications to generate large enough quantities of methane for clumped isotope analyses. For methane generation experiments all sources of P were removed and the medium was amended with methylphosphonic acid (aka MPn; Sigma-Aldrich, CAS Number 993-13-5) to a concentration of 2mM, with glucose (electron donor and carbon source) to a concentration of 3g/L, and sodium nitrate ($NaNO_3$) used as the terminal electron acceptor to a final concentration of 40mM. The growth medium was filter-sterilized then transferred to 160mL, 1 or 5L borosilicate bottles and vigorously degassed with ultra-high purity helium (UHP-He) for one hour per liter. Cell pellets from aerobic cultures were re-suspended and incubated on amended MPn and $NaNO_3$ media in 160mL butyl stoppered serum bottles. After reaching exponential phase on the MPn-amended media and positive head-space methane detection (via GC-FID), 1 or 5L cultures were inoculated to an optical density (OD600) of 0.001 and incubated at 30°C in the dark. Medium for D-enriched water experiments was prepared following the approach of Zhang and colleagues (Zhang et al., 2009), where it was enriched by adding a calculated quantity of D_2O (Sigma-Aldrich, CAS Number 7789-20-0) to the stock media prior to UHP-Helium flushing and sterilization.

The gaseous methane, dinitrogen, and carbon dioxide produced by strain HI00D01 were captured into gas-impermeable 0.25, 1, or 4L Tedlar bags, along with trace water vapor. The gas bags were built with straight thru 1/4 inch stainless steel tubing (GSB-P-1 Calibrated Instruments) to which we fitted with a 1/4 inch stainless steel needle valve by compression fitting to seal the gas bags before and after sample collection. To allow sample into the bag, we attached to the needle valve another 1/4" stub of stainless tubing, followed by a tube-to-pipe adapter 1/4" compression to 1/8" NPT,

followed by an 1/8" NPT to 1/4-28 adapter to then a luer lock and finally a threaded 18-G stainless steel dispensing needle (all plumbing parts from McMaster-Carr or Swagelok). The needle was inserted through black butyl stopper (GlasgerÃ€tebau Ochs GmbH) into the top of the bags through plastic funnels that were added for stability. At the end of the incubations, UHP-He sparged water was used to displace all remaining headspace into the Tedlar bags, allowed to equilibrate, then sealed by the needle valves and removed from experiment bottles, and the valves plugged with metal compression septa until preparation on the vacuum line.

3.2. Bulk isotope ratio measurements

Bulk carbon (δ^{13}C) and hydrogen (δD) isotope compositions of methylphosphonic acid (Sigma-Aldrich, CAS Number 993-13-5) were determined at the Northwestern University Stable Isotope Laboratory. Briefly, the δ^{13}C value of MPn was determined via EA-IRMS on a Costech 4010 Elemental Analyzer, coupled to a Delta V Plus isotope ratio mass spectrometer via a Conflo IV interface. Analyses were done in triplicate, and placed on the VPDB-LSVEC scale via analysis of organic standards supplied by Indiana University (acetanilide #1, urea #2a, and D-glucose) (Schimmelmann, 1991; Qi and Coplen, 2011). The bulk hydrogen (δD) isotope composition of MPn was determined via TC/EA-IRMS, operated at 1420°C, and coupled to a Delta V Plus isotope ratio mass spectrometer via a Conflo IV. Analyses were done in triplicate, and cross-referenced to the Ag-tube water isotope standards supplied by the USGS (GISP2, VSMOW, and UC03). The average composition of the non-exchangeable hydrogens on MPn (i.e., R-CH_3) was determined by equilibration with D-enriched waters (2mL) in a custom-designed vacuum chamber modified from a Costech zero-blank auto-sampler. Incubations were done at room temperature (25°C) for 6 days. At the end of the equilibration, water vapor was pumped to <50 mTorr for 2 hours, followed by subsequent TC/EA analyses with Ag-tube USGS standards as above, following published methods (Qi and Coplen, 2011).

Isotopic analysis of the medium water was conducted at the Stable Isotope Laboratory at Dartmouth College following published procedures (Kopec et al., 2019). Briefly, water hydrogen isotopic ratios (δD) were measured using the H-Device, in which water was reduced by hot chromium (850°C) and the resulting hydrogen gas was measured by an isotope ratio mass spectrometer (IRMS, Thermo Delta Plus XL). Isotopic ratios (D/H) are reported in

delta notation in permil (‰) deviation from the international standard VSMOW on the VSMOW-SLAP (Vienna Standard Mean Ocean Water, Standard Light Antarctic Precipitation) scale. The measurement 1σ uncertainty is 0.5‰ for δD, and the measured value was converted to the water isotope equivalent by calibration with known standards. When samples were presumed to be outside the range of the standards (e.g. for the enrichment experiments), samples were first diluted gravimetrically with a water standard of known composition. Uncertainty's due to dilution are accounted for and reported in Table 1 as the propagated 1se.

The stable isotopic compositions of methane samples generated by the C-P lyase in cultures of strain HI00D01 were measured on an ultra-high mass resolution isotope ratio mass spectrometer (Panorama, Nu Instruments) as part of the measurements to determine $\Delta^{12}CH_2D_2$ and $\Delta^{13}CH_3D$.

3.3. Multiply-substituted isotopologue measurements

The abundance of the two multiply-substituted mass-18 isotopologues of methane gas samples were measured on a Panorama (Nu Instruments) ultra-high-resolution gas-source isotope ratio mass spectrometer housed in the Department of Earth, Planetary, and Space Sciences at the University of California Los Angeles. Detailed descriptions of the mass spectrometry method were given by Young and colleagues (Young et al., 2016), and applied in recent studies (Young et al., 2017; Haghnegahdar et al., 2017; Giunta et al., 2019; Ash et al., 2019; Young, 2019).

Methane sample gases were purified on a vacuum line interfaced with a gas chromatograph (SRI GC-FID 8610) prior to isotopic analysis. This method was previously described in Young et. al (2016). Modification to the published procedures were as follows. The Tedlar gas bag holding the C-P lyase generated methane gas (mixed with UHP He, water vapor, and the other metabolic products N_2 and CO_2) was connected to the line with compression fittings and PTFE ferrules. Prior to gas introduction, the hydrocarbon-free vacuum line was evacuated to at least 4.0×10^{-7} mbar. Sample gas was introduced from the bag to the line in aliquots of 1000 mbar into a calibrated 50cc volume. Water vapor was trapped in a U-trap by ethanol-liquid nitrogen (LN_2) slurry at -80°C. The rest of the sample gas was then trapped on silica gel in a U-trap at LN_2 temperature for 10min, after which the non-condensable He was slowly pumped away. The methane aliquot was then cryofocused to remove the N_2 and CO_2 via GC and re-trapping on silica

gel as previously described (Young et al., 2017). Due to the significant partial pressure of N_2 relative to methane, and because complete separation of methane from N_2 was not achieved on the first pass through the GC, multiple aliquots were first passed though the GC, cryofocused, and co-trapped onto the same silica gel in a single glass cold-finger (6 to 7 GC-passes per sample bag). Once the requisite sample size of methane was captured (> 40 micromoles), the combined sample was once again cryofocused and passed through the GC a final time to remove trace N_2. The purified methane was then transferred to the Panorama inlet system for the bulk and clumped isotope ratio analyses following published protocols (Young et al., 2017).

3.4. Isotope notation

The isotopic compositions of carbon and hydrogen are reported as deviations from the carbon and hydrogen reference materials Vienna Peedee Belemnite and Vienna Standard Mean Ocean Water (VPDB and VSMOW, respectively). Standard delta notation is used to express the fractional differences:

$$\delta^{13}\mathrm{C} = 10^3 \left(\frac{(^{13}\mathrm{C}/^{12}\mathrm{C})_{\mathrm{sample}}}{(^{13}\mathrm{C}/^{12}\mathrm{C})_{\mathrm{VPDB}}} - 1 \right) \tag{7}$$

and

$$\delta\mathrm{D} = 10^3 \left(\frac{(\mathrm{D}/\mathrm{H})_{\mathrm{sample}}}{(\mathrm{D}/\mathrm{H})_{\mathrm{VSMOW}}} - 1 \right) \tag{8}$$

where all values are given in permil (‰), as shown. The relative abundances of the two multiply-substituted mass-18 isotopologues of methane are reported relative to the stochastic reference frame using the Δ_i notation, also in permil, where $\Delta^{13}CH_3D$ and $\Delta^{12}CH_2D_2$ are (Young et al., 2016):

$$\Delta^{13}\mathrm{CH_3D} = 10^3 \left(\frac{x(^{13}\mathrm{CH_3D})_{\mathrm{sample}}}{x(^{13}\mathrm{CH_3D})_{\mathrm{stochastic}}} - 1 \right) \tag{9}$$

and

$$\Delta^{12}\mathrm{CH_2D_2} = 10^3 \left(\frac{x(^{12}\mathrm{CH_2D_2})_{\mathrm{sample}}}{x(^{12}\mathrm{CH_2D_2})_{\mathrm{stochastic}}} - 1 \right), \tag{10}$$

respectively (Young et al., 2016). The stochastic fractional abundances of the mass-18 isotopologues are obtained from the measured bulk isotope fractional abundances of atoms in the sample such that

$$x(^{13}\mathrm{CH_3D})_{\mathrm{stochastic}} = 4\left(x(^{13}\mathrm{C})x(\mathrm{H})^3x(\mathrm{D})\right) \quad (11)$$

and

$$x(^{12}\mathrm{CH_2D_2})_{\mathrm{stochastic}} = 6\left(x(^{12}\mathrm{C})x(\mathrm{H})^2x(\mathrm{D})^2\right), \quad (12)$$

and where the coefficients of 4 and 6 account for the number of permutations for the positions of the D and H isotopes (Young et al., 2016).

4. Results

The isotopic compositions of methane produced from the degradation of MPn by strain HI00D01 in waters with different δD values in the range from -376 to $+6800$‰ are given in Table 1. The δD of product methane correlates closely with the δD of water (Figure 4). The methane δ^{13}C values vary little between -97 to -101‰ (mean = -99.9 ± 1.2 ‰, 1σ), closely tracking the δ^{13}C of the source MPn of near -100‰ relative to VPDB (Taenzer et al., 2020). The three non-exchangeable H-sites on the MPn methyl-group have a δD of -138 ± 5‰ relative to VSMOW for all of the experiments except those that utilized normal house water (-60‰, both B1 and B2). In the latter two experiments a different batch of MPn was used with the measured MPn methyl-group δD being -132 ± 5‰ relative to VSMOW. These results show that the final hydrogen added to the methyl-group derives from medium water during methane formation, and supports the recent finding that negligible carbon-isotope fractionation occurs during methane production from MPn via the C-P lyase pathway (Taenzer et al., 2020).

The measured $\Delta^{13}\mathrm{CH_3D}$ values of C-P lyase generated methane ranged between -0.29 and 0.934‰, with an average of $0.35 \pm 0.40\,1\sigma$ (Figure 5, Table 1). The variation in $\Delta^{13}\mathrm{CH_3D}$ values was only marginally greater than measurement uncertainties, and did not vary systematically with water δD, despite the significant contribution of water sourced from the medium with a range of δD values from -376 to $+6800$‰. In sharp contrast, the $\Delta^{12}\mathrm{CH_2D_2}$ values varied from -69.2 to $+7.1$‰, a spread much greater than measurement uncertainty of < 1‰ (Figure 5). The methane $\Delta^{12}\mathrm{CH_2D_2}$ values correlated closely with the medium water δD in a non-linear, semi-parabolic relationship (Figure 5).

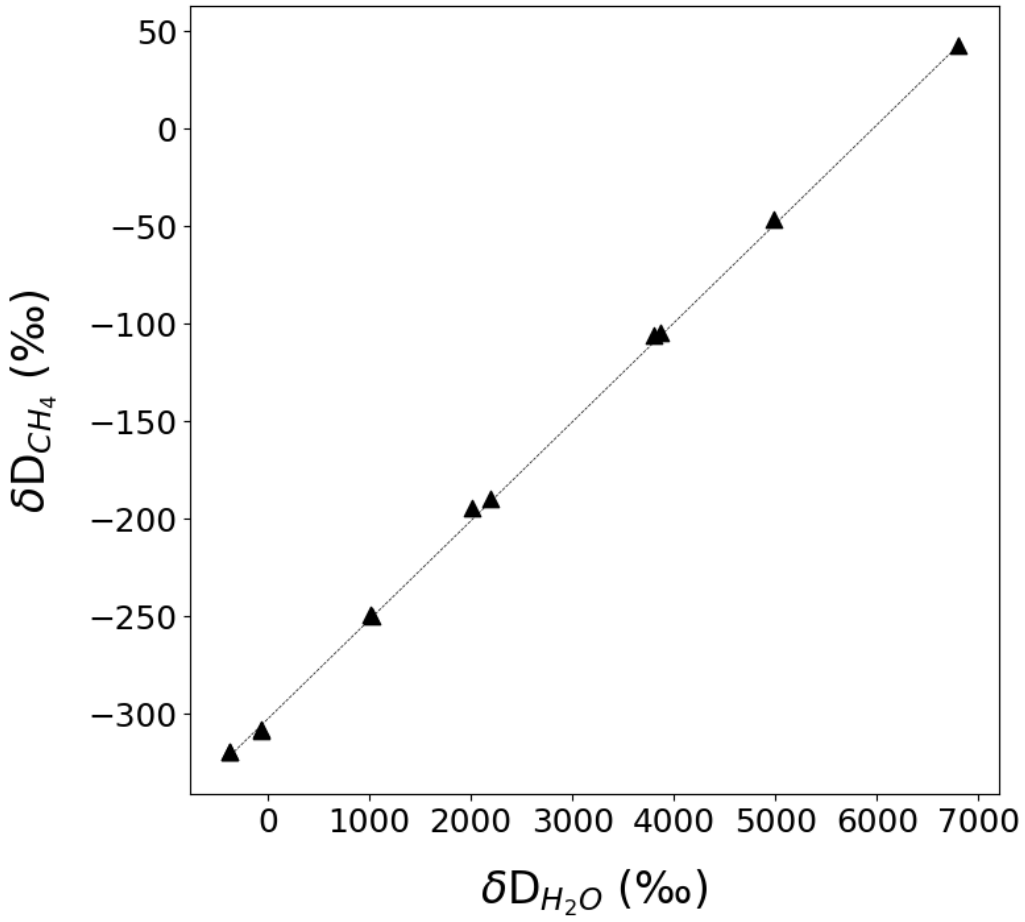

Figure 4: The D/H ratios of product methane vs. the D/H of medium water expressed in per mil deviations from VSMOW. Linear regression yields $\delta D_{CH_4} = 0.05\ \delta D_{H_2O} - 301.5$, with an R^2 of 0.999. The strong correlation betwen the isotopic ratios demonstrates addition of a consistent fraction of reactant water to product methane, and allows for the calculation of the fractionation factor between water D/H and the D/H of the single hydrogen added to the MPn CH_3 to form methane (see text).

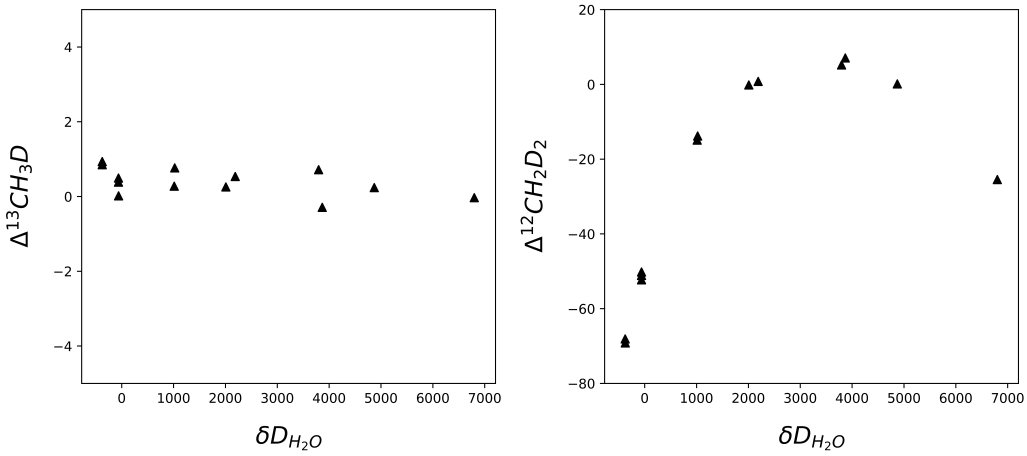

Figure 5: The measured (left) $\Delta^{13}CH_3D$ and (right) $\Delta^{12}CH_2D_2$ of microbialgenic methane produced in experiments with water of varying δD water for methane produced in various D-spiked experiments. Errors are smaller than the symbols.

Table 1: The isotopic compositions of medium waters and product methane.

Water			Methane							
Sample ID	δD	1se	δ^{13}C	1se	δD	1se	$\Delta^{13}CH_3D$	1se	$\Delta^{12}CH_2D_2$	1se
-400 B1	-376	0.5	-100.388	0.012	-319.26	0.04	0.93	0.35	-69.18	1.15
-400 B2	-376	0.5	-98.950	0.013	-319.22	0.04	0.85	0.44	-69.10	0.83
-60 B1	-63	0.5	-99.993	0.006	-299.49	0.04	0.02	0.13	-52.28	0.83
-60 B2	-63	0.5	-100.15	0.010	-300.22	0.03	0.50	0.24	-51.11	0.88
750 B1	1013	1.7	-97.047	0.006	-249.08	0.05	0.28	0.31	-14.90	1.32
750 B2	1022	7.3	-100.297	0.024	-250.12	0.05	0.77	0.42	-13.82	1.17
1500 B1	2007	5.1	-100.745	0.010	-194.72	0.04	0.26	0.18	-0.01	0.96
1500 B2	2188	5	-100.846	0.007	-190.06	0.04	0.54	0.27	0.79	1.11
3000 B1	3797	3.1	-100.213	0.009	-106.08	0.05	0.72	0.38	5.2	1.14
3000 B2	3868	2.3	-100.606	0.071	-104.59	0.06	-0.29	0.71	7.06	1.10
3900 B1+2	4871	7.9	-97.949	0.019	-46.43	0.03	0.24	0.36	0.12	0.72
5500 B1	6800	11.1	-100.480	0.006	42.39	0.04	-0.03	0.25	-25.46	0.85

5. Discussion

5.1. D/H fractionation between MPn and water

Understanding the sources of hydrogen used in methane formation by the C-P lyase enzyme is central to understanding the results of these experiments. The main substrate MPn is an organophosphonate synthesized by certain microbes in nature when faced with inorganic phosphate limitation (Metcalf et al., 2012; Yu et al., 2013). The methyl-group hydrogens on MPn

are ultimately derived from the water in which MPn is biosynthesized, offset by an unknown isotope effect. The hydrogen isotope fractionation between methyl-group hydrogens and water in more thoroughly studied processes, such as acetogenesis, show offsets from bulk water δD of hundreds of permil (Hattori et al., 2010). Here we utilized synthetic MPn with an average δD value distinct from all medium waters utilized (see Results). Phosphorus-starved microbes that encode the C-P lyase enzyme are able to grow on MPn as their sole source of phosphorus by breaking down MPn (Repeta et al., 2016; Sosa et al., 2019; Carini et al., 2014), and as a by-product, release methane (Kamat et al., 2011). The carbon-phosphorus bond in the methyl phosphonate intermediate, ribose-1-methylphosphonate 5-phosphate (PRPn), is attacked by the C-P lyase enzyme subunit PhnJ, producing ribose-1,2-cyclic-phosphate-5-phosphate (PRcP), and releasing the methyl group used to form methane. This reaction breaks the methyl group from the rest of the phosphonate compound. In vitro experiments with PhnJ showed that the hydrogen added to the methyl group originates from the bulk solvent (water) via a solvent exchangeable site on an amino acid in PhnJ (Kamat et al., 2011). The medium-derived hydrogen is delivered to form methane either by abstraction from the 5′-deoxyadenosine or the PhnJ amino acids. A representation of the overall reaction that underscores the sources of hydrogen from medium water and the MPn methyl group is

$$\mathrm{H_2O} + \overset{\mathrm{PRPn}}{[\mathrm{PO_4{-}C_5O_3H_8{-}PO_3{-}CH_3}]} + \overset{\mathrm{SAM}}{\mathrm{C_{15}H_{23}N_6O_5S}} \xrightarrow{\mathrm{PhnJ}} \overset{5'-\mathrm{deoxyadenosine}}{\mathrm{C_{10}H_{13}N_5O_3}} + \mathrm{OH} + \overset{\mathrm{PRcP}}{[\mathrm{PO_4{-}C_5O_2H_7{-}PO_4}]} + \overset{\mathrm{L-methionine}}{\mathrm{C_5H_{11}NO_2S}} + \mathrm{CH_4} \tag{13}$$

In our labelled water experiments, the methane δD increased with the water δD (Figure 4). Moreover, because we used the same lot of MPn for all reactions, with one exception that was isotopically similar (see *Results*), the methyl-group D/H was the same for all our experiments, and the increase in the D/H of product methane solely reflects the addition of water derived hydrogen with different D/H ratios. The tight correlation between bulk water and methane δD is described by the linear regression with an R^2 value of 0.999 (Figure 4). The regression equation is

$$\delta\mathrm{D}_{\mathrm{CH_4}} = 0.05\,\delta\mathrm{D}_{\mathrm{H_2O}} - 301.5. \tag{14}$$

The good correlation is consistent with the conclusion that methane is formed by transfer of a hydrogen from the medium water to the methyl group of MPn, and indicates that the transfer of hydrogen from water to the methyl group was consistent for all incubations in medium waters of different δD values. The slope in Equation 14 is the product of the fractionation factor between water and the hydrogen transferred to methane and the fraction of hydrogen in the methane derived from the water.

The good correlation described by Equation 14 is best explained as the result of constant fractions of hydrogen coming from the methyl group in MPn and water to produce methane. The most likely reason for this is that methane inherits 3/4 of its hydrogen directly from CH_3, and that water contributes the last hydrogen. The hydrogen isotope conservation equation for the formation of methane is therefore

$$0.75({}^{\mathrm{D}}R_{\mathrm{Methyl}}) + 0.25\,{}^{D}\alpha_{\mathrm{CH_4/H_2O}}({}^{\mathrm{D}}R_{\mathrm{H_2O}}) = {}^{\mathrm{D}}\,R_{\mathrm{CH_4}} \tag{15}$$

where ${}^{\mathrm{D}}R_i$ is the D/H ratio for species i. Using the known δD values for the product methane, medium water, and MPn methyl group from each experiment, the fractionation factor between methane and water, ${}^{\mathrm{D}}\alpha_{\mathrm{CH_4/H_2O}}$, for the one hydrogen transferred from water to make methane was determined by rearranging Equation 15, yielding:

$${}^{\mathrm{D}}\alpha_{\mathrm{CH_4/H_2O}} = \frac{4({}^{\mathrm{D}}R_{\mathrm{CH_4}} - (0.75\,{}^{\mathrm{D}}R_{\mathrm{Methyl}}))}{{}^{\mathrm{D}}R_{\mathrm{H_2O}}}. \tag{16}$$

The D/H fractionation factor between water and methane calculated from Equation 16 for the experiments with differing water δD values vary from 0.203 to 0.219 with an average value of 0.209 ± 0.005 1σ. The consistency is a reflection of the good correlation between δD values for CH_4 and H_2O (Figure 4). This fractionation factor corresponds to ${}^{\mathrm{D}}\varepsilon_{\mathrm{methane/water}} = -790 \pm 5$ ‰. The magnitude of fractionation between water and methane is relatively large, though not uncommon for processes involving hydrogen (Valentine et al., 2004; Kawagucci et al., 2014). However, the fractionation is not *a priori* outside the range for classical effects given the likelihood that it reflects a convolution of steps (i.e., product of fractination factors) involving D/H exchange on amino acids that accommodate the transfer of the last hydrogen that forms methane from water (Kamat et al., 2011). For this reason we do not attribute the magnitude of our derived fractionation factor to quantum tunneling. We note that because we know the D/H of the methyl group (ex-

changable hydrogen in MPn) and we can calculate the D/H of the hydrogen donated from water, we have characterized the D/H for the two sources of hydrogen drawn upon to construct the CH_4 molecules in each experiment.

The large isotope fractionation during the transfer of water hydrogen to the methyl group ensures that two compositionally distinct hydrogen reservoirs with distinct δD values contribute to product methane, one ultimately from medium water and the other from the methyl group in the MPn. Other mechanisms of methane formation that are analogous to the C-P lyase, such as microbial methylotrophic and acetotrophic methanogenesis (Penger et al., 2012), are likely influenced similarly. These metabolisms have been the target of recent investigations into their variance in $\Delta^{13}CH_3D$ in response to labelled substrate or water (Gruen et al., 2018), although $\Delta^{12}CH_2D_2$ values were not determined. In addition to these biogenic methane formation pathways, abiotic methane formation pathways where hydrogenated sites on end-product methane derive from two or more different reservoirs or with different fractionations from the source reservoir may be similarly influenced, as has been suggested (Yeung, 2016; Young et al., 2017; Young, 2019). Evidence of either quantum tunneling or the combinatorial effect were captured in methane generated at low-temperature via the abiotic Sabatier reaction, where a clear anti-clumped signal was observed in the $\Delta^{12}CH_2D_2$ with minimal variance in $\Delta^{13}CH_3D$ (Young et al., 2017). To determine if this was the combinatorial effect, future experiments with isotopically enriched molecular hydrogen are needed.

5.2. Effect of multiple D/H reservoirs on $\Delta^{12}CH_2D_2$

The combination of multiple reservoirs with distinct D/H ratios has a clear influence on the $\Delta^{12}CH_2D_2$ value of product methane. There was no corresponding effect on $\Delta^{13}CH_3D$ values. The negative $\Delta^{12}CH_2D_2$ values result from the nature of the clumped isotope reference frame. In general, when the stochastic distribution is calculated from a sample gas that averages different isotopic pools, negative Δ_i values result. By altering the isotopic composition of one of the two pools of hydrogen in the C-P lyase pathway, the medium water, we have apparently isolated this combinatorial effect on $\Delta^{12}CH_2D_2$.

In Figure 6, we illustrate the expected combinatorial effect on product methane for experiments like those reported here. When calculated $\Delta^{12}CH_2D_2$ values are plotted against the D/H isotopic composition of the water hydrogen isotopic composition where the methyl D/H is unchanged,

a parabolic trend emerges with an $\Delta^{12}CH_2D_2$ value near zero at the apex, whereas the $\Delta^{13}CH_3D$ is unchanged. This topology is predicted by the inequality in Equation 4 and has been demonstrated mathematically (Yeung et al., 2015; Yeung, 2016; Röckmann et al., 2016). As the isotopic composition of the hydrogens originating from the water and the methyl group diverge, the $\Delta^{12}CH_2D_2$ values become exponentially more negative. Negative values for $\Delta^{13}CH_3D$ do not emerge because of the unambiguous distinction between the $^{13}C/^{12}C$ and D/H ratios, yielding no ambiguity in the stochastic distribution (Figure 6).

5.3. Model for the observed $\Delta^{12}CH_2D_2$ effect

Our results resemble those expected for the combinatorial effect (compare Figures 5 and 6) and suggest that a combinatorial effect in $\Delta^{12}CH_2D_2$ is indeed manifest in at least one pathway for microbialgenic methane formation. In order to determine the extent to which the range of observed $\Delta^{12}CH_2D_2$ values is explained solely by the combinatorial effect we applied a model in which we calculate methane isotopologue abundances produced by a network of bi-molecular reactions between the isotopologues of the MPn methyl group and water, including the fractionation factor derived from Equation 16. The relative rates of the reactions were taken to be the product of the reactant relative concentrations. The eleven reactions comprising the model are

$$H_2O + {}^{12}CH_3 \rightarrow {}^{12}CH_4 + OH \quad (17)$$
$$H_2O + {}^{12}CH_2D \rightarrow {}^{12}CH_3D + OH \quad (18)$$
$$H_2O + {}^{12}CHD_2 \rightarrow {}^{12}CH_2D_2 + OH \quad (19)$$
$$HDO + {}^{12}CH_3 \rightarrow {}^{12}CH_4 + OD \quad (20)$$
$$HDO + {}^{12}CH_3 \rightarrow {}^{12}CH_3D + OH \quad (21)$$
$$HDO + {}^{12}CH_2D \rightarrow {}^{12}CH_3D + OD \quad (22)$$
$$HDO + {}^{12}CH_2D \rightarrow {}^{12}CH_2D_2 + OH \quad (23)$$
$$HDO + {}^{12}CHD_2 \rightarrow {}^{12}CH_2D_2 + OD \quad (24)$$
$$HDO + {}^{12}CHD_2 \rightarrow {}^{12}CHD_3 + OH \quad (25)$$
$$D_2O + {}^{12}CH_3 \rightarrow {}^{12}CH_3D + OD \quad (26)$$
$$D_2O + {}^{12}CH_2D \rightarrow {}^{12}CH_2D_2 + OD. \quad (27)$$

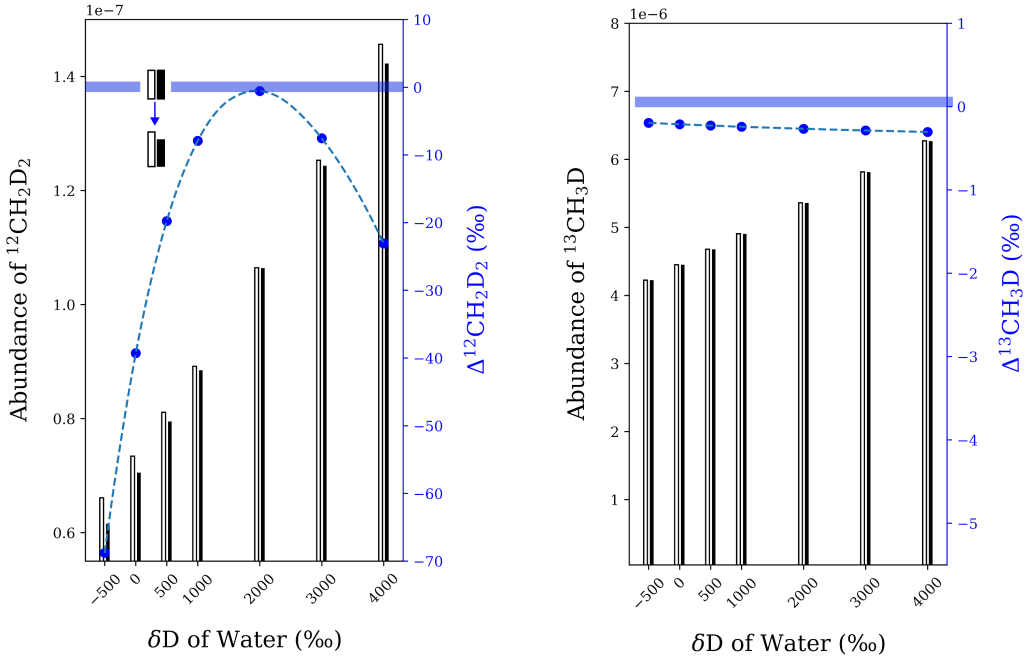

Figure 6: An illustration of the difference between the stochastic abundances of $\Delta^{12}CH_2D_2$ and $\Delta^{13}CH_3D$ predicted when using average isotopic compositions of the sample gas versus the isotopic compositions of the specific reactants. The abundance of the clumped isotopologues that results from the δD and δ^{13}C in any given methane population is shown by the white bars, whereas, the abundance of the clumped isotopologues predicted from using the isotopic composition of the specific reservoirs, water and MPn, is given in the black bars, and correspond to the left Y-axes. The clumped isotope values are depicted by the blue dashed line, and correspond to the right Y-axes. If the isotopic composition of the source reservoirs that contribute to product methane have the same δD values, then the clumped values will not vary, shown by the horizontal blue bar at zero in each panel. In reality, the clumped isotopic compositions are negative across most water δD values (assuming an invariant methyl-group), because the stochastic isotopologue abundance using the average C and H isotopic composition of the sample gas is greater than that given by the isotopic composition of the methyl group and water. All points in this plot are illustrative and not real data.

We also used an analogous set of reactions in which the ^{13}C-bearing isotopologues of the methyl group were included. The rate of reaction was modified by the fractionation factor from Equation 16 where a D in CH_4 comes from water. We performed the calculations for values of ${}^{D}\alpha_{CH_4/H_2O}$ ranging from 0.19 to 0.23 in order to allow for uncertainties in the precise value.

We performed the calculations in two ways. In the first calculation, we assumed that the reactants had stochastic relative abundances of isotopologues calculated from their measured bulk δ^{13}C and δD values. From the relative rates of reaction we calculate the resulting abundances of the methane isotopologues and the $\Delta^{12}CH_2D_2$ and $\Delta^{13}CH_3D$ values expected for each incubation experiment.

The fit of the model curves obtained using purely stochastic reactant isotopologue abundances is sufficiently good (Figure 7) that we conclude that the combinatorial effect is the dominant process governing the values for $\Delta^{12}CH_2D_2$ in the product methane. However, there is a marked offset between the model curves and the measured values at higher water δD values. As expected, the calculations, produce $\Delta^{13}CH_3D$ within $< 0.2‰$, signifying no effect on $\Delta^{13}CH_3D$, as observed in our experiments.

In our second calculation method, we obtained an improved fit to the data by considering that the reactant methyl group did not have a purely stochastic distribution of isotopologues. Specifically, we allowed for a higher concentration of CHD_2 relative to stochastic. In order to determine a best-fit value for the reactant methyl clumping, we adjusted the ratio $CHD_2/(CHD_2)_{stochastic}$ to minimize the chi-square calculated from the deviation in $\Delta^{12}CH_2D_2$ values between the data and the model. For this minimization we adopted the mean ${}^{D}\alpha_{CH_4/H_2O}$ value of 0.209. The results yield a best-fit $CHD_2/(CHD_2)_{stochastic}$ ratio of 1.0114 that can be expressed as a $\Delta^{12}CHD_2$ value of 11.4‰ (Figure 7). For a nominal reproducibility of ±2‰ for $\Delta^{12}CH_2D_2$ values implied by some of the replicate experimental results in Table 1, the reduced chi-square value for the fit of this model is 2.5 (for n = 12 experiments). This value is sufficiently close to unity to suggest that the vast majority of the variation exhibited by our data is due to the combinatorial effect that includes inheritance of a modest amount of DD clumping from the reactant methyl group in MPn.

In order to assess the importance of the analytical uncertainties in the two input parameters for our calculations, we performed Monte Carlo (MC) simulations of the experiments by randomly varying the MPn methyl-group δD values and the ${}^{D}\alpha_{CH_4/H_2O}$ values in our model calculations at the water

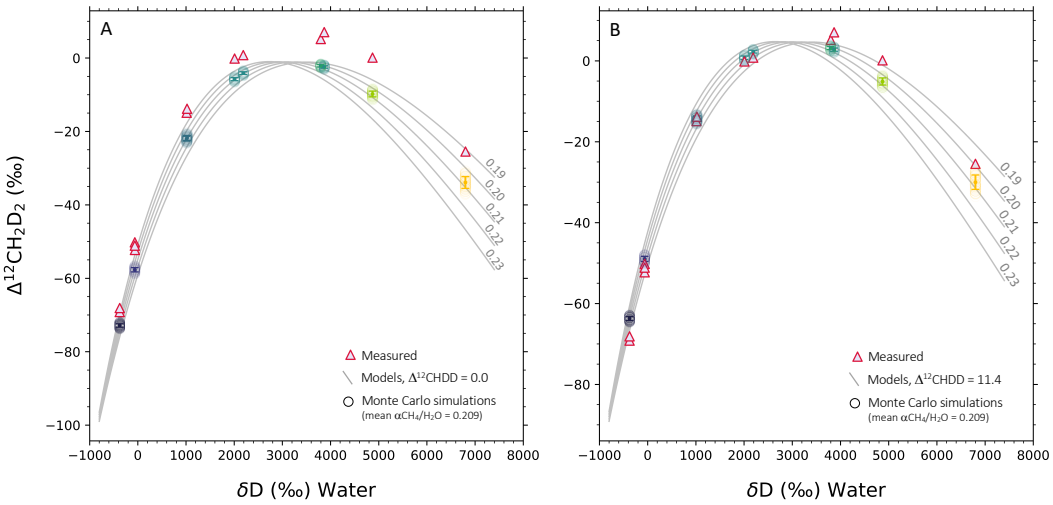

Figure 7: Plots of $\Delta^{12}CH_2D_2$ vs. water δD showing our experimental results (triangles) and the two model calculations described in the text (curves). The model curves in panel A assume stochastic distributions for all of the reactant isotopologues. The model curves in panel B are obtained using a best-fit $\Delta^{12}CHD_2$ value of 11.4‰ for the reactant methyl group (see text). Curves for a range of ${}^{D}\alpha_{CH_4/H_2O}$ values from 0.19 to 0.23 are shown for reference. Monte Carlo simulations of the effects of uncertainties in MPn methyl δD and our derived ${}^{D}\alpha_{CH_4/H_2O}$ values are shown by the circles. Means and standard deviations for the Monte Carlo simultaions are shown by the filled circle and 1σ vertical error bars.

δD values corresponding to the experiments. We drew 100 random instances of these values from parent Gaussian distributions based on the measured means and standard deviations for these parameters and used these as inputs to the calculations. The resulting MC estimates for the uncertainties in the models are shown in both panels in Figure 7. For the 7 groups of experiments representing 7 distinct δD water values, 6 have measured $\Delta^{12}CH_2D_2$ values that are within the 4σ uncertainty in our best-fit model with $\Delta^{12}CHD_2 = 11.4‰$ (panel B, Figure 7).

Our best-fit model allows us to not only simulate the combinatorial effect on the product methane, but it also affords an estimate of the DD clumping in the MPn methyl group that produced the methane. The value for $\Delta^{12}CHD_2$ in this instance reflects the process of forming reagent MPn. Experiments similar to these might be useful in exploring the DD ordering in naturally occurring MPn methyl groups.

5.4. Implications for applications of $\Delta^{12}CH_2D_2$

Negative $\Delta^{12}CH_2D_2$ values have been attributed to either combinatorial effects or quantum tunneling effects (Young et al., 2017; Young, 2019). The results of this study lend support to the interpretation that combinatorial effects dominate. These effects may arise from enzymatically-mediated kinetic steps within a cell or surface catalyzed steps during abiotic synthesis. In both cases we refer to these as endogenous combinatorial effects because they are the result of distinct pools of hydrogen created by the kinetic steps leading to methane formation. In the present study, the pools of contrasting D/H ratios arise in part because of the isotopic composition of the growth medium, comprising what we refer to as an example of exogenous combinatorial effects to emphasize that the pools of hydrogen with distinct D/H ratios include an external reservoir. Endogenous combinatorial effects may explain the very low $\Delta^{12}CH_2D_2$ values seen in microbial methanogenesis and in abiotic Sabatier reaction products (Young et al., 2017; Young, 2019).

A critical advantage of using $\Delta^{12}CH_2D_2$ and $\Delta^{13}CH_3D$ values to characterize the provenance of methane molecules is their relative insensitivity to substrate bulk isotopic compositions (Young et al., 2017; Young, 2019). For example, the very negative $\Delta^{12}CH_2D_2$ values that are characteristic of, or even diagnostic of, microbialgenic methane appear to be insensitive to the δD of the local aqueous environs (Young et al., 2017; Young, 2019; Ash et al., 2019). However, the strong response of $\Delta^{12}CH_2D_2$ values to the isotopic composition of water in these experiments raises the specter of substrate bulk

isotope effects on methane $\Delta^{12}CH_2D_2$ values. Though some of the experimental water values were not representative of natural systems (e.g. δD_{H_2O} > 0‰), both the Hanover, NH, USA (house) and South Pole, Antarctica waters represent values for reservoirs in nature that can contribute hydrogen to methane. We note that the more than 300‰ difference in the δD of the two waters resulted in a more than 15‰ shift in methane $\Delta^{12}CH_2D_2$ values at a fixed substrate MPn isotopic composition (Figure 5). The likelihood for such effects in nature depends on the variability of D/H in natural waters and variability in fractionation factors between water and the natural methyl-type substrates used in methanogenesis. For the step-wise addition of hydrogen to carbon during hydrogenotrophic (H_2 + CO_2) methanogenesis, where all of the hydrogen for the product methane ultimately originates from water, endogenous combinatorial effects likely dominate due to the different D/H fractionation factors associated with each hydrogen addition step (Young, 2019). This said, if some of the hydrogens on methane come from molecular hydrogen (Valentine et al., 2004; Kawagucci et al., 2014), the opportunity for combinaotiral influence arises. Indeed, the other canonical microbial pathways of methane formation, methylotrophic or acetotrophic, are clear analogs to the C-P lyase pathway, in that different D/H pools are accessed in the form of water and preexisting methyl groups, suggesting that exogenous combinatorial effects are at play. This is especially true given the likelihood for large D/H fractionations between water and C-H bearing organic sources of H in nature (Hattori et al., 2010), without which reservoir (exogenous) combinatorial effects are unlikely. More work is required to understand whether or not differences in $\Delta^{12}CH_2D_2$ values among different methanogenesis pathways (Giunta et al., 2019; Young et al., 2017) could in part reflect the different magnitudes of endogenous and exogenous combinatorial effects.

6. Conclusions

The source of depleted $\Delta^{12}CH_2D_2$ values in methane produced by microbes is evidenced in the aerobic C-P lyase pathway. This metabolism for methane production incorporates hydrogen from two distinct reservoirs: a methyl group, contributing three hydrogenated sites, and water that donates a single hydrogen. By varying the D/H composition of the water medium in which the bacteria generate methane, we observed the effect of combinatorics on $\Delta^{12}CH_2D_2$ values. Our results indicate that variations in the $\Delta^{12}CH_2D_2$ of

methane produced by C-P lyase is primarily the result of the difference in D/H between the water and the reactant methyl group. The consistency between predictions for the purely combinatorial reservoir effect and the measured isotopologue abundances demonstrates that in this case, combinatorics are the main cause of the negative $\Delta^{12}CH_2D_2$ values with no resolvable effect on $\Delta^{13}CH_3D$ values for the product methane. These results lend credence to the interpretation that combinatorial effects dominate the depleted microbialgenic methane $\Delta^{12}CH_2D_2$ values as well as those those arising from some surface catalyzed abiotic methane production pathways. This work raises the prospect that differential water H-isotopic compositions or fractionations in nature may induce the combinatorial effect in some microbial methane production pathways.

Acknowledgements

Funding was provided by the Simons Foundation (WDL), the NASA NH Space Grant NNX15AH79 (WDL, LT), and the Sloan Foundation Deep Carbon Observatory (EDY); we thank Beverly Chiu and Alec Cobban for laboratory assistance.

Research Data

All code for model and figures is posted in a permanent archive FigShare DOI: 10.6084/m9.figshare.11676357

References

Ash, J., M. Egger, T. Treude, I. Kohl, B. Cragg, R. Parkes, C. Slomp, B. Sherwood Lollar, and E. Young (2019). Exchange catalysis during anaerobic methanotrophy revealed by $^{12}CH_2D_2$ and $^{13}CH_3D$ in methane. *Geochemical Perspectives Letters*, 26–30.

Cao, X., H. Bao, and Y. Peng (2019). A kinetic model for isotopologue signatures of methane generated by biotic and abiotic co2 methanation. *Geochimica et Cosmochimica Acta 249*, 59–75.

Carini, P., A. E. White, E. O. Campbell, and S. J. Giovannoni (2014). Methane production by phosphate-starved SAR11 chemoheterotrophic marine bacteria. *Nature Communications 5*, 1–7.

615 Eiler, J. M. and E. Schauble (2004). $^{18}O^{13}C^{16}O$ in Earths atmosphere.
616 *Geochimica et Cosmochimica Acta 68*, 4767–4777.

617 Giunta, T., E. D. Young, O. Warr, I. Kohl, J. L. Ash, A. Martini, S. O. Mun-
618 dle, D. Rumble, I. Pérez-Rodríguez, M. Wasley, D. E. LaRowe, A. Gilbert,
619 and B. Sherwood Lollar (2019). Methane sources and sinks in continen-
620 tal sedimentary systems: New insights from paired clumped isotopologues
621 13CH3D and 12CH2D2. *Geochimica et Cosmochimica Acta 245*, 327–351.

622 Gruen, D. S., D. T. Wang, M. Könneke, B. D. Topçuoğlu, L. C. Stewart,
623 T. Goldhammer, J. F. Holden, K.-U. Hinrichs, and S. Ono (2018). Ex-
624 perimental investigation on the controls of clumped isotopologue and hy-
625 drogen isotope ratios in microbial methane. *Geochimica et Cosmochimica*
626 *Acta 237*, 339–356.

627 Haghnegahdar, M. A., E. A. Schauble, and E. D. Young (2017). A model
628 for 12CH2D2 and 13CH3D as complementary tracers for the budget of
629 atmospheric CH4. *Global Biogeochemical Cycles 31*(9), 1387–1407.

630 Hattori, R., K. Yamada, H. Shibata, S. Hirano, O. Tajima, and N. Yoshida
631 (2010). Measurement of the isotope ratio of acetic acid in vinegar by hs-
632 spme-gc-tc/c-irms. *Journal of Agricultural and Food Chemistry 58*(12),
633 7115–7118. PMID: 20504023.

634 Kamat, S. S., H. J. Williams, L. J. Dangott, M. Chakrabarti, and F. M.
635 Raushel (2013). The catalytic mechanism for aerobic formation of methane
636 by bacteria. *Nature 497*(7447), 132–136.

637 Kamat, S. S., H. J. Williams, and F. M. Raushel (2011). Intermediates
638 in the transformation of phosphonates to phosphate by bacteria. *Na-*
639 *ture 480*(7378), 570–573.

640 Kawagucci, S., M. Kobayashi, S. Hattori, K. Yamada, Y. Ueno, K. Takai, and
641 N. Yoshida (2014). Hydrogen isotope systematics among h2–h2o–ch4 dur-
642 ing the growth of the hydrogenotrophic methanogen methanothermobac-
643 ter thermautotrophicus strain δh. *Geochimica et Cosmochimica Acta 142*,
644 601–614.

645 Kopec, B., X. Feng, E. Posmentier, and L. Sonder (2019). Seasonal deuterium
646 excess variations of precipitation at summit, greenland, and their climato-

logical significance. *Journal of Geophysical Research: Atmospheres 124*(1), 72–91.

Metcalf, W. W., B. M. Griffin, R. M. Cicchillo, J. Gao, S. C. Janga, H. A. Cooke, B. T. Circello, B. S. Evans, W. Martens-Habbena, D. A. Stahl, and W. A. van der Donk (2012). Synthesis of Methylphosphonic Acid by Marine Microbes: A Source for Methane in the Aerobic Ocean. *Science 337*(6098), 1104–1107.

Penger, J., R. Conrad, and M. Blaser (2012). Stable Carbon Isotope Fractionation by Methylotrophic Methanogenic Archaea. *Applied and Environmental Microbiology 78*(21), 7596–7602.

Popa, M. E., D. Paul, C. Janssen, and T. Röckmann (2019). H_2 clumped isotope measurements at natural isotopic abundances. *Rapid Communications in Mass Spectrometry 33*(3), 239–251.

Qi, H. and T. B. Coplen (2011). Investigation of preparation techniques for δ^2H analysis of keratin materials and a proposed analytical protocol. *Rapid Communications in Mass Spectrometry 25*(15), 2209–2222.

Repeta, D. J., S. Ferrón, O. A. Sosa, C. G. Johnson, L. D. Repeta, M. Acker, E. F. Delong, and D. M. Karl (2016). Marine methane paradox explained by bacterial degradation of dissolved organic matter. *Nature Geoscience 9*(12), 884–887.

Röckmann, T., M. E. Popa, M. C. Krol, and M. E. G. Hofmann (2016). Statistical clumped isotope signatures. *Scientific Reports 6*(1), 31947.

Schimmelmann, A. (1991). Determination of the concentration and stable isotopic composition of nonexchangeable hydrogen in organic matter. *Analytical chemistry 63*(21), 2456–2459.

Sosa, O. A., D. J. Repeta, E. F. DeLong, M. D. Ashkezari, and D. M. Karl (2019, may). Phosphate limited ocean regions select for bacterial populations enriched in the carbon–phosphorus lyase pathway for phosphonate degradation. *Environmental Microbiology*, 1462–2920.14628.

Stolper, D. A., M. Lawson, C. L. Davis, A. A. Ferreira, E. V. S. Neto, G. S. Ellis, M. D. Lewan, A. M. Martini, Y. Tang, M. Schoell, A. L. Sessions, and

J. M. Eiler (2014). Formation temperatures of thermogenic and biogenic methane. *Science 344*(6191), 1500–1503.

Taenzer, L., P. Carini, A. Masterson, B. Bourque, J. Gaube, and W. Leavitt (2020). Microbial methane from methylphosphonate isotopically records source. *Geophysical Research Letters 47*(1), e2019GL085872.

Valentine, D. L. (2011). Emerging Topics in Marine Methane Biogeochemistry. *Annual Review of Marine Science 3*(1), 147–171.

Valentine, D. L., A. Chidthaisong, A. Rice, W. S. Reeburgh, and S. C. Tyler (2004). Carbon and hydrogen isotope fractionation by moderately thermophilic methanogens 1 1Associate editor: N. E. Ostrom. *Geochimica et Cosmochimica Acta 68*(7), 1571–1590.

Wang, D. T., D. S. Gruen, B. S. Lollar, K.-U. Hinrichs, L. C. Stewart, J. F. Holden, A. N. Hristov, J. W. Pohlman, P. L. Morrill, M. Konneke, K. B. Delwiche, E. P. Reeves, C. N. Sutcliffe, D. J. Ritter, J. S. Seewald, J. C. McIntosh, H. F. Hemond, M. D. Kubo, D. Cardace, T. M. Hoehler, and S. Ono (2015, apr). Nonequilibrium clumped isotope signals in microbial methane. *Science 348*(6233), 428–431.

White, A. K. and W. W. Metcalf (2004). Two C-P Lyase Operons in Pseudomonas stutzeri and Their Roles in the Oxidation of Phosphonates, Phosphite, and Hypophosphite. *Journal of Bacteriology 186*(14), 4730–4739.

Yeung, L. Y. (2016). Combinatorial effects on clumped isotopes and their significance in biogeochemistry. *Geochimica et Cosmochimica Acta 172*, 22–38.

Yeung, L. Y., J. L. Ash, and E. D. Young (2015). Biological signatures in clumped isotopes of O2. *Science 348*(6233), 431–434.

Yeung, L. Y., S. Li, I. E. Kohl, J. A. Haslun, N. E. Ostrom, H. Hu, T. P. Fischer, E. A. Schauble, and E. D. Young (2017). Extreme enrichment in atmospheric 15n15n. *Science advances 3*(11), eaao6741.

Young, E. (2019). A two-dimensional perspective on ch4 isotope clumping: Distinguishing process from source. In O. B. N., I. Daniel, and R. Dasgupta (Eds.), *Deep Carbon Past to Present*, pp. 388–414. Cambridge: Cambridge University Press.

Young, E., I. Kohl, B. S. Lollar, G. Etiope, D. Rumble, S. Li, M. Haghnegahdar, E. Schauble, K. McCain, D. Foustoukos, C. Sutclife, O. Warr, C. Ballentine, T. Onstott, H. Hosgormez, A. Neubeck, J. Marques, I. Pérez-Rodríguez, A. Rowe, D. LaRowe, C. Magnabosco, L. Yeung, J. Ash, and L. Bryndzia (2017). The relative abundances of resolved 12CH2D2 and 13CH3D and mechanisms controlling isotopic bond ordering in abiotic and biotic methane gases. *Geochimica et Cosmochimica Acta 203*, 235–264.

Young, E. D., D. Rumble, P. Freedman, and M. Mills (2016). A large-radius high-mass-resolution multiple-collector isotope ratio mass spectrometer for analysis of rare isotopologues of O_2, N_2, CH_4 and other gases. *International Journal of Mass Spectrometry 401*, 1–10.

Yu, X., J. R. Doroghazi, S. C. Janga, J. K. Zhang, B. Circello, B. M. Griffin, D. P. Labeda, and W. W. Metcalf (2013). Diversity and abundance of phosphonate biosynthetic genes in nature. *Proceedings of the National Academy of Sciences 110*(51), 20759–20764.

Zhang, X., A. L. Gillespie, and A. L. Sessions (2009). Large D/H variations in bacterial lipids reflect central metabolic pathways. *Proceedings of the National Academy of Sciences 106*(31), 12580–12586.